Inorg. Chem. **2005**, *44*, 5447−5458

Controlled Synthesis of Ternary II−II′−VI Nanoclusters and the Effects of Metal Ion Distribution on Their Spectral Properties

Marty W. DeGroot,[†] Nicholas J. Taylor,[‡] and John F. Corrigan*[,†]

Departments of Chemistry, The University of Western Ontario, London, Canada N6A 5B7, and University of Waterloo, Waterloo, Canada N2L 3G1

Received December 30, 2004

The reaction of $[(3,5\text{-}Me_2\text{-}C_5H_3N)_2Zn(ESiMe_3)_2]$ (E = Se, Te) with cadmium(II) acetate in the presence of $PhESiMe_3$ and P^nPr_3 at low temperature leads to the formation of single crystals of the ternary nanoclusters $[Zn_xCd_{10-x}E_4(EPh)_{12}(P^nPr_3)_4]$ [E = Se, x = 1.8 (**2a**), 2.6 (**2b**); Te, x = 1.8 (**3a**), 2.6 (**3b**)] in good yield. The clusters $[Zn_3Hg_7Se_4(SePh)_{12}(P^nPr_3)_4]$ (**4**) and $[Cd_{3.7}Hg_{6.3}Se_4(SePh)_{12}(P^nPr_3)_4]$ (**5**) can be accessed by similar reactions involving $[(3,5\text{-}Me_2\text{-}C_5H_3N)_2Zn(SeSiMe_3)_2]$ or [(*N*,*N*′-tmeda)Cd(SeSiMe$_3$)$_2$] (**1**) and mercury(II) chloride. The metal silylchalcogenolate reagents are efficient delivery sources of $\{ME_2\}$ in cluster synthesis, and thus, the metal ion content of these clusters can be readily moderated by controlling the reaction stoichiometry. The reaction of cadmium acetate with $[(3,5\text{-}Me_2\text{-}C_5H_3N)_2Zn(SSiMe_3)_2]$, $PhSSiMe_3$, and P^nPr_3 affords the larger nanocluster $[Zn_{2.3}Cd_{14.7}S_4(SPh)_{26}(P^nPr_3)_2]$ (**6**). The incorporation of Zn(II) into $\{Cd_{10}E\}$ (E = Se, Te) and Zn(II) or Cd(II) into $\{Hg_{10}Se\}$ nanoclusters results in a significant blue shift in the energy of the first "excitonic" transition. Solid-state thermolysis of complexes **2** and **3** reveals that these clusters can be used as single-source precursors to bulk ternary $Zn_xCd_{1-x}E$ materials as well as larger intermediate clusters and that the metal ion ratio is retained during these reactions.

Introduction

Clusters and colloids of II−VI semiconductors continue to attract considerable research attention due to their potential uses in materials[1] and biological[2] applications. The unique optical and electronic properties demonstrated by these quantum-confined particles (quantum dots or QDs) can be attributed to the change in the electronic structure with particle size, a phenomenon not observed in bulk materials or molecular solids.[3] The majority of synthetic research in this area has thus been focused on the controlled modulation of crystallite size and the reduction of polydispersity.[4−7] A further area of concentration focuses on shape-controlled II−VI nanomaterials with recently reported structures comprising nanowires, nanocables, nanoribbons, and nanorods, among others.[8−10] There are relatively few reports involving

* Author to whom correspondence should be addressed. E-mail: corrigan@uwo.ca. Phone: (+1)519-661-2111. Fax: (+1)519-661-3022.
† The University of Western Ontario.
‡ University of Waterloo.

(1) (a) Klein, D. L.; Roth, R.; Lim, A. K. L.; Alivisatos, A. P.; McEuen, P. L. *Nature* **1997**, *389*, 699−701. (b) Colvin, V. L.; Schlamp, M. C.; Alivisatos, A. P. *Nature* **1994**, *370*, 354−357. (c) Radloff, C.; Moran, C. E.; Jackson, J. B.; Halas, N. J. *Mol. Nanoelectron.* **2003**, 229−262. (d) Willner, I.; Willner, B. *Pure Appl. Chem.* **2002**, *74*, 1773−1783. (e) Kershaw, S. V.; Harrison, M. T.; Burt, M. G. *Philos. Trans. R. Soc. London, Ser. A* **2003**, *361*, 331−343. (f) Feldheim, D. L.; Keating, C. D. *Chem. Soc. Rev.* **1998**, *28*, 1−12.

(2) (a) Michalet, X.; Kapanidis, A. N.; Laurence, T.; Pinaud, F.; Doose, S.; Pflughoefft, M.; Weiss, S. *Ann. Rev. Biophys. Biomol. Struct.* **2003**, *32* 161−182. (b) Lacoste, T. D.; Michalet, X.; Pinaud, F.; Chemla, D. S.; Alivisatos, A. P.; Weiss, S. *Proc. Natl. Acad. Sci. U.S.A.* **2000**, *97*, 9461−9466. (d) Bruchez, M.; Moronne, M.; Gin, P.; Weiss, S.; Alivisatos, A. *Science* **1998**, *281*, 2013−2015. (d) Chan, W. C.; Nie, S. *Science* **1998**, *281*, 2106−2018.

(3) For reviews see: (a) Alivisatos, A. *J. Phys. Chem.* **1996**, *100*, 13226−13239. (b) Weller, H. *Angew. Chem., Int. Ed. Engl.* **1993**, *32*, 41−53. (c) Murray, C. B.; Kagan, C. R.; Bawendi, M. G. *Annu. Rev. Mater. Sci.* **2000**, *30*, 545−610. (d) Steigerwald, M. L.; Brus, L. E. *Acc. Chem. Res.* **1990**, *23*, 183−188. (e) Efros, A. L.; Rosen, M. *Annu. Rev. Mater. Sci.* **2000**, *30*, 475−521. (f) Henglein, A. *Chem. Rev.* **1989**, *89*, 1861−1873.

(4) Murray, C. B.; Norris, D. J.; Bawendi, M. G. *J. Am. Chem. Soc.* **1993**, *115*, 8706−8715.

(5) (a) Murray, C. B.; Kagan, C. R.; Bawendi, M. G. *Science* **1995**, *270*, 1335−1338. (b) Katari, J. E. B.; Colvin, V. L.; Alivisatos, A. P. *J. Phys. Chem.* **1994**, *98*, 4109−4117.

(6) (a) Peng, Z. A.; Peng, X. *J. Am. Chem. Soc.* **2002**, *124*, 3343−3353. (b) Peng, Z. A.; Peng X. *J. Am. Chem.* Soc. **2001**, *123*, 1389−1395. (c) Ou, L.; Peng, Z. A.; Peng X. *Nano Lett.* **2001**, *1*, 333−337.

(7) (a) Katari, J. E. B.; Colvin, V. L.; Alivisatos, A. P. *J. Phys. Chem.* **1994**, *98*, 4109−4117. (b) Peng, X.; Wickham, J.; Alivisatos, A. P. *J. Am. Chem. Soc.* **1998**, *120*, 5343−5344. (c) Manna, L.; Scher, E. C.; Alivisatos, A. P. *J. Am. Chem. Soc.* **2000**, *122*, 12700−12706.

(8) (a) Peng, X. G.; Manna, L.; Yang, W. D.; Wickham, J.; Scher, E.; Kadavanich, A.; Alivisatos, A. *Nature* **2000**, *404*, 59−63. (b) Tang, K.; Qian, Y.; Zeng, Z.; Yang, X. *Adv. Mater.* **2003**, *15*, 448−450.

(9) Liu, Y.; Xu, Y.; Li, J.-P.; Zhang, B.; Wu, D.; Sun, Y.-H. *Chem. Mater.* **2004**, *33*, 1162−1163.

10.1021/ic0481576 CCC: $30.25
Published on Web 06/22/2005

the preparation of ternary II−II′−VI nanomaterials.[11−13] In these alloyed compounds, manipulation of the band gap energy can be achieved by changing both particle size and composition (i.e. the ratio of M to M′). Recently, this has been demonstrated with the synthesis of a series highly of luminescent $Zn_xCd_{1-x}Se$ nanocrystals whose emission energy can be tuned across the visible spectrum by increasing the Zn:Cd ratio.[13] Thus, the development of new approaches to access ternary nanoparticles is an attractive pursuit.

Semiconductor nanocluster materials whose structures can be determined crystallographically are of significant interest from the perspective that they allow an investigation of the development of materials properties from the molecular size regime.[14] This is particularly relevant in reference to cluster molecules of II−VI semiconductors because many of these complexes are built from the same structural units that comprise bulk crystalline and nanocrystalline semiconductors.[14,15] Thus, these clusters can be regarded as molecular models for these larger systems. This analogy was cemented by a recent investigation of the optical properties of a series of structurally characterized CdSe clusters ranging from molecular $[Cd_4(SePh)_6Cl_4]^{2-}$ to the nanocluster $[Cd_{32}Se_{14}(SePh)_{36}(P^nPr_3)_4]$.[16] In this report, it was demonstrated that the absorption and emission features of these clusters can be correlated with those observed for larger nanoparticles and the quantum confinement effects observed for CdSe nanoparticles could be extended to these molecules.

The area of metal chalcogen cluster chemistry has continued to emerge in nanomaterials science, attributable in part to the advent of the use of silylated chalcogen reagents. The reagents $E(SiMe_3)_2$ and $RESiMe_3$ (E = S, Se, Te) offer a convenient and effective route for the delivery of E^{2-} and RE^-, respectively, in the synthesis of semiconductor nanoclusters.[14−19] The "tunability" of the "R" group in the latter affords the opportunity to easily control the nature of the capping ligands, and this can have a profound influence on the products observed.[20] In addition, these reagents are readily adaptable to introduce specific chemical functionality into the cluster architecture. The synthesis of the complex $Fe(\eta^5\text{-}C_5H_4SeSiMe_3)_2$ and the monosilylated counterpart $(\eta^5\text{-}C_5H_5)Fe(\eta^5\text{-}C_5H_4SeSiMe_3)$ has yielded a route for the introduction of redox-active ferrocenyl units onto group 11 and group 12 metal selenolate clusters, respectively.[21,22] Similarly, the design of metal−chalcogenolate complexes with reactive $[S(SiMe_2S)_2^{2-}]$[23] or $[E(SiMe_3)^-]$ (E = S, Se, Te)[24−26] functionalities offers a powerful entry into high-nuclearity ternary cluster and nanocluster materials. Metal−chalcogenolate reagents for the controlled incorporation of the heavier congeners, Se and Te, are particularly difficult to access due to the reactivity of these chalcogen elements.

Recently, we developed an approach to ternary II−II′−VI nanoclusters via the silylated chalcogenolate complexes $[(N,N'\text{-tmeda})Zn(ESiMe_3)_2]$ and their use in the synthesis of the ternary II−II′−VI nanoclusters $[(N,N'\text{-tmeda})_5Zn_5Cd_{11}E_{13}(EPh)_6]$.[27] The chelating *N*,*N*′-tmeda ligands constrain the Zn centers to reside at the surface of the nanocluster, and thus, the cluster can be viewed as the molecular limit of a core/shell nanoparticle. This approach has been expanded to the synthesis of II−II′−VI clusters wherein the metal ions M and M′ are intimately mixed within the cluster core.[28] Herein we report on the synthesis, structure, and optical properties of a series of ternary ZnCdE (E = S, Se, Te), ZnHgSe, and CdHgSe clusters.

(10) Ma, C.; Ding, Y.; Moore, D.; Wang, X.; Wang, Z. L. *J. Am. Chem. Soc.* **2004**, *126*, 708−709.

(11) (a) Wang, W.; Germanenko, I.; El-Shall, M. S. *Chem. Mater.* **2002**, *14*, 3028−3033. (b) Korgel, B. A.; Monbouquette, H. G. *Langmuir* **2000**, *16*, 3588−3594. (c) Petrov, D. V.; Santos, B. S.; Pereira, G. A. L.; Donegá, C. D. M. *J. Phys. Chem. B* **2002**, *106*, 5325−5334. (d) Harrison, M. T.; Kershaw, S. V.; Burt, M. G.; Eychmüller, A.; Weller, H.; Rogach, A. L. *Mater. Sci. Eng. B* **2000**, *69*, 355−360. (e) Rogach, A. L.; Harrison, M. T.; Kershaw, S. V.; Kornowski, A.; Burt, M. G.; Eychmüller, A.; Weller, H. *Phys. Status Solidi B* **2001**, *224*, 153−158.

(12) Zhong, X.; Liu, S.; Zhang, Z.; Li, L.; Wei, Z.; Knoll, W. *J. Mater. Chem.* **2004**, 2790−2794.

(13) (a) Zhong, X.; Han, M.; Dong, Z.; White, T. J.; Knoll, W. *J. Am. Chem. Soc.* **2003**, *125*, 8589−8594. (b) Zhong, X.; Zhang, Z.; Liu, S.; Han, M.; Knoll, W. *J. Phys. Chem. B* **2004**, *108*, 15552−15559.

(14) Corrigan, J. F.; DeGroot, M. W. *The Chemistry of Nanomaterials: Synthesis, Properties and Applications*; Rao, C. N. R., Müller, A., Cheetham, A. K., Eds.; Wiley-VCH: Weinheim, Germany, 2004; Vol. 2, pp 418−451.

(15) (a) DeGroot, M. W.; Corrigan, J. F. *Comprehensive Coordination Chemistry II*; Fujita, M., Powell, A., Creutz, C., Eds.; Pergamon: Oxford, U.K., 2004; Vol. 7, pp 57−123. (b) Dance, I.; Fisher, K. *Prog. Inorg. Chem.* **1994**, *41*, 637−803.

(16) Solviev, V. N.; Eichhöfer, A.; Fenske, D.; Banin, U. *J. Am. Chem. Soc.* **2001**, *123*, 2354−2364.

(17) For reviews see: (a) Dehnen, S.; Eichhöfer, A.; Fenske, D. *Eur. J. Inorg. Chem.* **2002**, 279−317. (b) Fenske, D.; Corrigan, J. F. *Metal Clusters in Chemistry*; Braunstein, P., Oro, L. A., Raithby, B., Eds.; Wiley-VCH: Weinheim, Germany, 1999; Vol. 3, Chapter 4.2, pp 1302−1324.

(18) (a) Fenske, D.; Ohmer, J.; Hachgenei, J. *Angew. Chem., Int. Ed. Engl.* **1985**, *24*, 993−995. (b) Dehnen, S.; Fenske, D. *Chem.*—Eur. J. **1996**, 2, 1407−1416. (c) Zhu, N.; Fenske, D. *J. Chem. Soc., Dalton Trans.* **1999**, 1067−1075. (d) Corrigan, J. F.; Fenske, D. *Angew. Chem., Int. Ed. Engl.* **1997**, *36*, 1981−1983. (e) Eichhöfer, A.; Fenske, D. *J. Chem. Soc., Dalton Trans.* **1998**, 2969−2972. (f) Bettenhausen, M.; Eichhöfer, A.; Fenske, D.; Semmelmann, M. *Z. Anorg. Allg. Chem.* **1999**, *625*, 593−601. (g) Deveson, A.; Dehnen, S.; Fenske, D. *J. Chem. Soc., Dalton Trans.* **1997**, 4491−4498. (h) Fenske, D.; Krautscheid, H. *Angew. Chem.* **1990**, *29*, 1452−1454. (i) Fenske, D.; Zhu, N.; Langetepe, T. *Angew. Chem., Int. Ed.* **1998**, *37*, 2640−2644. (j) Wang, X.-J.; Langetepe, T.; Persau, C.; Kang, B.-S.; Sheldrick, G. M.; Fenske, D. *Angew. Chem., Int. Ed.* **2002**, *41*, 3818−3820. (k) Langetepe, T.; Fenske, D. *Angew. Chem., Int. Ed.* **2002**, *41*, 300−304.

(19) (a) Krautscheid, H.; Fenske, D.; Baum, G.; Semmelmann, M. *Angew. Chem., Int. Ed. Engl.* **1993**, *32*, 1303−1305. (b) Fenske, D.; Persau, C.; Dehnen, S.; Anson, C. E. *Angew. Chem., Int. Ed.* **2004**, *43*, 305−309.

(20) Corrigan, J. F.; Fenske, D. *Chem. Commun.* **1997**, 1837−1838. (b) Corrigan, J. F.; Balter, S.; Fenske, D. *J. Chem. Soc., Dalton Trans.* **1996**, 729−735.

(21) (a) Wallbank, A. I.; Corrigan, J. F. *Chem. Commun.* **2001**, 377−378. (b) Wallbank, A. I.; Corrigan, J. F. *J. Cluster Sci.* **2004**, *15*, 225−232.

(22) Lebold, T. P.; Stringle, D. L. B.; Workentin, M. S.; Corrigan, J. F. *Chem. Commun.* **2003**, 1398−1399.

(23) (a) Komuro, T.; Matsuo, T.; Kawaguchi, H.; Tatsumi, K. *Angew. Chem., Int. Ed.* **2003**, *42*, 465−468. (b) Komuro, T.; Matsuo, T.; Kawaguchi, H.; Tatsumi, K. *Chem. Commun.* **2002**, 988−989.

(24) Tran, D. T. T.; Taylor, N. J.; Corrigan, J. F. *Angew. Chem., Int. Ed.* **2000**, *39*, 935−937.

(25) Tran, D. T. T.; Beltran, L. M. C. B.; Kowalchuk, C. M.; Trefiak, N. R.; Taylor, N. J.; Corrigan, J. F. *Inorg. Chem.* **2002**, *41*, 5693−5698.

(26) Komuro, T.; Matsuo, T.; Kawaguchi, H.; Tatsumi, K. *J. Chem. Soc., Dalton Trans.* **2004**, 1618−1625.

(27) (a) DeGroot, M. W.; Taylor, N. J.; Corrigan, J. F. *J. Am. Chem. Soc.* **2003**, *125*, 864−865. (b) DeGroot, M. W.; Taylor, N. J.; Corrigan, J. F. *J. Mater. Chem.* **2004**, 654−660.

(28) DeGroot, M. W.; Corrigan, J. F. *Angew. Chem.* **2004**, *43*, 5355−5357.

Experimental Section

Materials and Methods. Standard Schlenk techniques and gloveboxes were employed for all synthetic and handling procedures. The solvents THF, toluene, pentane, hexane, and heptane were dried and collected using an MBraun MB-SP Series solvent purification system with tandem activated alumina (tetrahydrofuran) or activated alumina/activated copper redox catalyst (hydrocarbons).[29] Dichloromethane-d_2 and THF-d_8 were purchased from Cambridge Isotope Laboratories. The precursor complexes [(3,5-Me_2-$C_5H_3N)_2Zn(ESiMe_3)_2$] (E = S, Se, Te) were prepared according to the procedures described previously.[30] Cadmium acetate was purchased as the dihydrate (Strem) and dried in vacuo at 135 °C for 12 h. The reagents $PhESiMe_3$ (E = S, Se, Te)[31−33] and P^nPr_3[34] were synthesized according to literature procedures. $^{31}P\{^1H\}$ nuclear magnetic resonance spectra were measured using a Varian Inova 400 spectrometer with an operating frequency of 161.957 MHz. Chemical shifts were reported in ppm and were referenced externally to 85% H_3PO_4. Ultraviolet−visible spectra were recorded on a Varian Cary 100 Bio UV−vis spectrophotometer. Solid-phase diffuse reflectance spectra were measured on the same instrument using an auxiliary module. Samples were diluted in anhydrous KBr. Solution photoluminescence spectra were measured at 77 K on a SPEX Fluorolog II spectrofluorometer using a HgXe excitation lamp. Thermogravimetric analyses (TGA) and single differential thermal analyses (SDTA) were carried out using a Mettler Toledo TGA/SDTA851^e instrument. Volatile decomposition products were transferred via nickel tubing to a Varian CP-3800 gas chromatograph with a Varian Saturn 2000 GC/MS/MS mass spectrometer as the detector. Powder X-ray diffraction (PXRD) patterns were obtained on a Rigaku diffractometer with Co Kα radiation source (λ = 1.799 260 Å). Dynamic light scattering experiments were carried out with a Malvern Zetasizer Nano S series particle size analyzer with a He−Ne laser (633 nm) and avalanche photodiode photon detector. Solvents and samples were filtered through 0.02 μm Anotop 10 inorganic membrane filters (Whatman) prior to analysis. EDX analyses were carried out by Mr. Ross Davidson at Surface Science Western (UWO). An EDAX Phoenix model energy dispersive X-ray (EDX) system with light element detection capability was used to obtain semiquantitative analysis of Zn, Cd, Se, Te, and P. The instrument was coupled to a Hitachi S-4500 scanning electron microscope (SEM). Analyses were carried out using a 20 kV electron beam focused on single crystals of the samples and repeated to ensure reproducibility. Atomic absorption spectroscopy (AAS) measurements were carried out using a Varian SpectrAA flame atomic absorption spectrometer. Samples were prepared by decomposition of the clusters in concentrated HNO_3 followed by dilution to 0.1 M HNO_3 such that the zinc and cadmium concentrations would fall within the range of the respective standard curve. The standard solutions were of $Zn(NO_3)_2$ and $Cd(NO_3)_2$ dissolved in 0.1 M HNO_3. The concentrations of the standards were 0, 0.5, 1, 2, 5, and 10 ppm Zn and Cd. Metal content was determined by linear regression to data from the standards. Chemical analyses were performed by Chemisar Laboratories Inc. (Guelph, Ontario, Canada).

[(*N*,*N*′-tmeda)$Cd(SeSiMe_3)_2$], 1. A solution of cadmium(II) acetate (0.20 g, 0.87 mmol) and TMEDA (0.20 mL, 1.30 mmol) was prepared in 15 mL of THF. The reaction was cooled to −78 °C, at which temperature the (*N*,*N*′-tmeda)$Cd(OAc)_2$ adduct precipitates out of solution. Bis(trimethylsilyl)selenide (0.37 mL, 1.73 mmol) was added at −78 °C, and the reaction was allowed to warm slowly to −40 °C, where a clear, colorless solution was obtained. The complex could not be isolated; however, the complete conversion of starting reagents to product was determined by in situ NMR experiments in both THF-d_8 and CD_2Cl_2. ^1H NMR (CD_2Cl_2, 193 K, δ): 2.79 (s, br, N−CH_2), 2.38 (s, br, N−CH_3), 0.33 (s, $SiMe_3$). $^{13}C\{^1H\}$ NMR (CD_2Cl_2, 193 K, δ): 55.97 (s, N−CH_2), 44.86 (s, N−CH_3), 6.46 (s, $SiMe_3$). ^{29}Si NMR (CD_2Cl_2, 193 K, δ): 6.6. $^{77}Se\{^1H\}$ NMR (CD_2Cl_2, 193 K, δ): −534.

[$Zn_{1.8}Cd_{8.2}Se_4(SePh)_{12}(P^nPr_3)_4$], 2a. A solution of [(3,5-Me_2-$C_5H_3N)_2Zn(SeSiMe_3)_2$] in 20 mL of THF at −78 °C was prepared. The THF was removed cold in vacuo and replaced with 40 mL of cold (−78 °C) toluene. This solution was added to a solution of cadmium(II) acetate (1.51 g, 6.54 mmol) and P^nPr_3 (3.25 mL, 16.4 mmol) in toluene (150 mL) at −78 °C. $PhSeSiMe_3$ (2.45 mL, 0.98 mmol) was then added, and the reaction was allowed to warm slowly to room temperature yielding a pale yellow solution. Cluster **2a** could be isolated by precipitation with 100 mL of heptane, filtering out, and drying under vacuum. Single crystals suitable for X-ray analysis were obtained by overlayering the reaction solution with heptane. Yield of crystalline **2a**: 2.38 g (67.9%). Anal. Calcd: C, 33.52; H, 3.75. Found: C, 33.60; H, 3.63. Metal ion stoichiometry given by AAS (Chemisar): $Zn_{1.9}Cd_{8.1}$. Metal ion content given by AAS analysis: Cd, 22.03 ± 0.61%; Zn, 2.62 ± 0.14%; yielding a metal stoichiometry of $Zn_{1.7}Cd_{8.3}$. Atomic ratios given by EDX analysis: $Zn_{1.8}Cd_{8.2}Se_{14.7}P_{3.0}$. $^{31}P\{^1H\}$ NMR (CD_2Cl_2, 295 K, δ): −12.8 (s, br, Cd−P^nPr_3), −21.1 (s, br, Zn−P^nPr_3).

[$Zn_{2.6}Cd_{7.4}Se_4(SePh)_{12}(P^nPr_3)_4$], 2b. Cluster **2b** was prepared in the same manner as for **2a**, with cadmium(II) acetate (1.51 g, 6.54 mmol) and P^nPr_3 (3.25 mL, 16.40 mmol) in toluene (150 mL) at −78 °C with the exception that the amount of [(3,5-Me_2-$C_5H_3N)_2$-$Zn(SeSiMe_3)_2$] was increased (2.28 mmol) with a corresponding decrease in $PhSeSiMe_3$ (2.11 mL, 8.46 mmol). Pure, crystalline **2b** was precipitated from solution with heptane, filtered out, and dried. Single crystals for X-ray structural characterization were obtained in the same manner as for **2a**. Yield: 2.54 g (75.6%). Anal. Calcd: C, 33.80; H, 3.79. Found: C, 33.12; H, 3.75. Metal ion stoichiometry given by AAS (Chemisar): $Zn_{2.4}Cd_{7.6}$. Atomic ratios given by EDX analysis: $Zn_{2.7}Cd_{7.3}Se_{15.3}P_{3.2}$. $^{31}P\{^1H\}$ NMR (CD_2Cl_2, 295 K, δ): −12.8 (s, br, Cd−P^nPr_3), −21.1 (s, br, Zn−P^nPr_3).

[$Zn_{1.8}Cd_{8.2}Te_4(TePh)_{12}(P^nPr_3)_4$], 3a. Cadmium (II) acetate (1.00 g, 4.34 mmol) was dissolved in THF (100 mL) with P^nPr_3 (2.1 mL, 10.8 mmol). The solution was cooled to −78 °C and added to a freshly prepared solution of [(3,5-Me_2-$C_5H_3N)_2Zn(TeSiMe_3)_2$] (1.08 mmol) with excess 3,5-lutidine at the same temperature. The resulting pale yellow solution was immediately treated with $PhTeSiMe_3$ (1.49 mL, 6.51 mmol) producing a bright yellow solution. Upon warming slowly to room temperature, a yellow solution was obtained. The addition of heptane (100 mL) produced a very pale yellow precipitate, which was filtered out to remove the mother liquor, washed with pentane, and dried in vacuo. Alternatively, single crystals were obtained by overlayering the reaction solution with heptane. Yield: 1.67 g (66.8%). Anal. Calcd: C, 27.97; H, 3.13. Found: C, 27.72; H, 3.16. Metal ion stoichiometry given by AAS (Chemisar): $Zn_{1.6}Cd_{8.4}$. Atomic ratios

(29) Pangborn, A. B.; Giardello, M. A.; Grubbs, R. H.; Rosen, R. K.; Timmers, F. J. *Organometallics* **1996**, *15*, 1518−1520.
(30) Degroot, M. W.; Corrigan, J. F. *Organometallics*, in press.
(31) Bruynes, C. A.; Jurriens, T. K. *J. Org. Chem.* **1982**, *47*, 3966−3969.
(32) Detty, M. R.; Seidler, M. D. *J. Org. Chem.* **1981**, *46*, 1283−1292.
(33) Jones, C. H. W.; Sharma, R. D. *J. Organomet. Chem.* **1984**, *268*, 113−118.
(34) Cumper, C. W. N.; Foxton, A. A.; Read, J.; Vogel, A. I. *J. Chem. Soc.* **1964**, 430−434.

given by EDX analysis: $Zn_{1.8}Cd_{8.2}Te_{14.7}P_{3.6}$. $^{31}P\{^1H\}$ NMR (CD_2Cl_2, 295 K, δ): −20.9 (s, br, Cd−P^nPr_3), −25.4 (s, br, Zn−P^nPr_3).

$[Zn_{2.6}Cd_{7.4}Te_4(TePh)_{12}(P^nPr_3)_4]$, 3b. Cluster **3b** was formed in the same manner as **3a**, with cadmium(II) acetate (1.51 g, 6.54 mmol) and P^nPr_3 (3.25 mL, 16.40 mmol) in toluene (150 mL) at −78 °C but using 1.52 mmol of $[(3,5\text{-}Me_2\text{-}C_5H_3N)_2Zn(TeSiMe_3)_2]$ and 5.64 mmol (1.29 mL) of $PhTeSiMe_3$. Pure, crystalline **3b** could be precipitated from solution with heptane and isolated after filtration and drying in vacuo or could be crystallized by layering with heptane. Yield: 1.90 g (70.4%). Anal. Calcd: C, 28.14; H, 3.15. Found: C, 28.92; H, 3.02. Metal ion content given by AAS analysis: Cd, 18.26 ± 0.65%; Zn, 3.26 ± 0.14%; yielding a metal stoichiometry of $Zn_{2.5}Cd_{7.5}$. Atomic ratios given by EDX analysis: $Zn_{2.6}Cd_{7.4}Te_{13.5}P_{3.2}$. $^{31}P\{^1H\}$ NMR (CD_2Cl_2, 295 K, δ): −20.9 (s, br, Cd−P^nPr_3), −25.4 (s, br, Zn−P^nPr_3).

$[Zn_3Hg_7Se_4(SePh)_{12}(P^nPr_3)_4]$, 4. A solution of mercury(II) chloride (0.30 g, 1.09 mmol) and P^nPr_3 (0.43 mL, 2.18 mmol) in toluene (30 mL) was cooled to −78 °C and then added to a freshly prepared solution containing $[(3,5\text{-}Me_2\text{-}C_5H_3N)_2Zn(SeSiMe_3)_2]$ (0.38 mmol) and $PhSeSiMe_3$ (0.35 mL, 1.42 mmol). The addition immediately produced a pale yellow solution which darkened within a few minutes to deep yellow and then pale orange. After being allowed to stir at −78 °C for 15 min, the reaction solution was layered with 40 mL of cold heptane and stored at −80 °C overnight. The reaction was warmed slowly by storage at −25 °C overnight and then finally being allowed to warm to room temperature in an ice bath. A small number of bright yellow crystals formed at the solvent interface, and a small amount of black precipitate was observed; however, the reaction solution remained bright yellow. Mixing of the solvent layers produced a bright yellow crystalline precipitate. After 1 day, a large number of bright yellow crystals of **4** suitable for X-ray crystallography formed on the side of the flask, along with another small amount of black solid. Complex **4** was isolated by transferring the crystals by pipet to a second flask, followed by repeated washing with hexane to remove the amorphous precipitate. The crystals were then dried under vacuum. Isolated yield: 0.18 g (32.4%). Anal. Calcd: C, 29.28; H, 3.28. Found: C, 29.61; H, 3.00. Atomic ratios given by EDX analysis: $Zn_{3.0}Hg_{7.0}Se_{18.3}P_{3.7}$.

$[Cd_{3.7}Hg_{6.3}Se_4(SePh)_{12}(P^nPr_3)_4]$, 5. Mercury(II) chloride (0.296 g, 1.09 mmol) was dissolved in toluene (30 mL) with 2 equiv of P^nPr_3 (0.43 mL, 2.18 mmol), and the solution was cooled to −78 °C. This solution was then transferred to a freshly prepared solution containing $[(N,N'\text{-tmeda})Cd(SeSiMe_3)_2]$ (0.38 mmol) and $PhSeSiMe_3$ (0.35 mL, 1.42 mmol) in 10 mL of THF, also at −78 °C. The solution immediately turned bright yellow. The reaction was allowed to warm slowly to −25 °C overnight, and the solution darkened to a deep yellow. The solution was layered with 30 mL of cold heptane, and the reaction flask was stored undisturbed in the dark at 4 °C. After 2 days at this temperature, bright orange single crystals had formed amidst a large amount of red/brown precipitate. The crystals were transferred by pipet, washed several times with hexane to remove the precipitate, and dried in vacuo. Isolated yield: 0.03 g (6.5%). Anal. Calcd: C, 28.76; H, 3.22. Found: C, 29.65; H, 3.02. Metal stoichiometry given by AAS (Chemisar): $Cd_{3.8}Hg_{6.2}$. Atomic ratios given by EDX analysis: $Cd_{3.7}Hg_{6.3}Se_{18.3}P_{4.4}$.

$[Zn_{2.3}Cd_{14.7}S_4(SPh)_{26}(P^nPr_3)_2]$, 6. Cadmium(II) acetate (0.30 g, 1.30 mmol) was dissolved in 30 mL of toluene with the addition of P^nPr_3 (0.97 mL, 4.88 mmol). The solution was cooled to −78 °C and added to a similarly cooled slightly turbid solution of $[(3,5\text{-}Me_2\text{-}C_5H_3N)_2Zn(SSiMe_3)_2]$ (0.24 g, 0.36 mmol) in 6 mL of THF. The reaction was stirred for 15 min at −78 °C and was then treated with $PhSSiMe_3$ (0.35 mL, 1.87 mmol) and allowed to warm slowly. After 90 min, a clear, colorless solution was obtained, and the reaction was allowed to warm to room temperature overnight. Single crystals suitable for X-ray analysis were grown by layering the reaction solution with heptane (20 mL). Yield: 0.19 g (38.4%). Anal. Calcd: C, 40.94; H, 3.40. Found: C, 39.28; H, 3.21. Atomic ratios given by EDX analysis: $Zn_{2.3}Cd_{14.7}S_{25}P_{2.2}$.

X-ray Structural Characterization. Single crystals of compounds **2**−**6** of suitable quality for X-ray analysis were carefully selected from large collections of crystals that were immersed in polyfluoropolyether oil or paraffin oil (Aldrich). The coated crystals were mounted on either a glass fiber or nylon fiber "hoop" attached to the goniometer head, with the oil setting upon cooling in a flow of cold N_2. The X-ray diffraction data for complexes **2**, **3**, and **5** were collected at 200 K using graphite-monochromated Mo $K\alpha_1$ radiation ($\lambda = 0.710\ 73$ Å) on a Nonius Kappa-CCD diffractometer. Intensity data were collected using the software COLLECT (Nonius, 1998). Nonius DENZO software was used for crystal cell refinement and data reduction, while scaling was performed using Nonius SCALE-PACK. Data for **4** and **6** were measured at 150 K on an Oxford Cryostream equipped Bruker SMART APEX CCD diffractometer (University of Waterloo) with the same radiation source. Intensity data were collected using Bruker SMART software (version 4.05, Bruker AXS Inc., Madison, WI, 1996), while SAINT software (version 4.05, Bruker AXS Inc., Madison, WI, 1996) was used for cell refinement and data reduction. Data for all compounds were corrected for Lorentz and polarization effects. Structures for all complexes were solved using direct methods program and refined on F_o^2 data using the full-matrix least-squares method program of the SHELXTL (G. M. Sheldrick, Madison, WI) program package. The weighting scheme was of the form $w = 1/[\sigma^2(F_o^2) + (aP)^2 + bP]$ (a, b = refined variables, $P = {}^1/_3 \max(F_o^2, 0) + {}^2/_3F_c^2$). For complexes **2a** and **3b** all non-hydrogen atoms were refined anisotropically, while for **4**−**5** heavy atoms (Zn, Cd, Hg, P, Se) were refined anisotropically with carbon atoms refined isotropically. Hydrogen atoms were included in **2**, **3**, and **5** as riding on their respective carbon atoms. For cluster **6**, diffraction data was weak and the structure could only be satisfactorily refined in the chiral space group $I2$. The atomic positions of the respective carbon atoms of the P^nPr_3 and −SPh groups were grouped and refined collectively using free variables. Cadmium atoms were refined anisotropically, while S, P, and C atoms (including those of two toluene molecules) were refined isotropically. Hydrogen atoms were not included. Molecular diagrams were prepared using the SHAKAL 99 drawing program.[35]

Solid-State Thermolysis of the Clusters. Solid-state thermal decomposition was carried out on crystalline samples of complexes **2a**,**b** and **3a**,**b** under a stream of nitrogen in the TGA analyzer. Samples were placed in a 150 μL platinum crucible heated at a rate of 15 °C/min to the desired final temperature and then maintained at that temperature for 30 min. The volatile decomposition products were identified by GC/MS via "on-line" transfer of the TGA purge gas to a sample preconcentration trap (SPT) on the GC instrument. Solid residues were collected and stored under nitrogen for further analysis.

Results and Discussion

Synthesis, Composition, and Structural Characterization of the Ternary Nanoclusters. The synthesis of metal

(35) Keller, E. *SCHAKAL 1999, A Computer Program for the Graphic Representation of Molecular and Crystallographic Models*; Universität Freiburg: Freiburg, Germany, 1999.

Table 1. Crystallographic Data and Parameters for Complexes **2**−**6**

param	**2a**	**3b**	**4**	**5**	**6**
formula[a]	$C_{108}H_{144}P_4Zn_{1.2}Cd_{8.8}Se_{16}$	$C_{108}H_{144}P_4Zn_2Cd_8Te_{16}$	$C_{108}H_{144}P_4Hg_{10}Se_{16}$	$C_{108}H_{144}P_4Cd_4Hg_6Te_{16}$	$C_{174}H_{172}P_2Cd_{17}S_{30}$
fw	3897.04	4637.65	4835.37	4570.80	5289.43
cryst system	tetragonal	tetragonal	cubic	cubic	monoclinic
space group	$I4_1/a$	$I4_1/a$	$F\bar{4}3c$	$I\bar{4}3m$	$I2$
temp (K)	200(2)	200(2)	150(2)	200(2)	150(2)
a (Å)	25.3442(5)	25.9100(2)	37.1143(12)	18.6251(5)	34.2588(2)
b (Å)	25.3442(5)	25.9100(2)	37.1143(12)	18.6251(5)	35.932(2)
c (Å)	20.2084(6)	21.6000(2)	37.1143(12)	18.6251(5)	35.100(2)
α (deg)	90	90	90	90	90
β (deg)	90	90	90	90	90.239(2)
γ (deg)	90	90	90	90	90
V (Å^3)	12980.4(5)	14500.7(2)	51124(3)	6460.0(3)	43208(4)
μ(Mo Kα_1) (mm^{-1})	6.205	4.709	16.610	13.363	1.980
Z	4	4	16	2	8
ρ_{calcd} (g cm^{-3})	1.994	2.124	2.513	2.350	1.571
reflcns collcd	14 327	16 307	58 308	1915	145 399
indpndt reflcns	7449	8298	3776	1093	75 212
R_{int}	0.0831	0.0348	0.1220	0.0345	0.0778
R indices	$R_1 = 0.0525$	$R_1 = 0.0309$	$R_1 = 0.0695$	$R_1 = 0.0412$	$R_1 = 0.1067$
$[I > 2\sigma(I)]$[b]	$wR_2 = 0.1104$	$wR_2 = 0.0779$	$wR_2 = 0.1636$	$wR_2 = 0.1111$	$wR_2 = 0.2538$

[a] The ambiguity between the metal compositions determined from analytical methods (AAS, EDX, and elemental analyses) and those obtained from X-ray crystallographic data can be attributed to the difficulty in assigning with certainty low occupancies for M′ in the crystallographic model. While these data were valuable in providing information regarding the location of the metal sites with highest M′ occupancy, more confidence was placed in the ratios obtained from the other analytical means. [b] $R_1 = \Sigma||F_o| - |F_c||/\Sigma|F_o|$. $wR_2 = \{\Sigma[w(F_o^2 - F_c^2)^2/\Sigma[w[F_o^2]^2]^{1/2}$.

chalcogenolate complexes with terminal trimethylsilyl functionalities offers a powerful route for the production of ternary MM′E nanoclusters.[24−28] The preformed metal−chalcogen bond combined with the inherent reactivity of −ESiMe$_3$ groups toward metal halide or acetate salts ensures the essential formation of M−E−M′ bonding interactions during cluster growth. The synthesis of (trimethylsilyl)-chalcogenolate complexes of zinc(II) has been reported recently.[27,28,30] This chemistry has been extended to the formation of (*N*,*N*′-tmeda)Cd(SeSiMe$_3$)$_2$, **1** (eq 1). It is found that complex **1** is not stable for extended periods in solution even at low temperature and decomposes readily to bright-yellow polynuclear CdSe species via the elimination of Se(SiMe$_3$)$_2$. The instability of these complexes versus the zinc derivatives[30] can be attributed to the relative strength of the M−N interaction, which is expected to be stronger in the case of zinc. These observations are in agreement with the reported sensitivity of polymeric "[Cd(SeSiMe$_3$)$_2$]$_\infty$".[36] Attempts to isolate crystalline **1** have to this point proven unsuccessful, as this invariably results in the formation of intractable solids that could not be dissolved in organic solvents. These results suggest that the removal of solvent results in the formation of polynuclear or polymeric CdSe compounds. Similarly, attempts at synthesizing [(3,5-Me$_2$-C$_5$H$_3$N)$_2$Cd(SeSiMe$_3$)$_2$] from [(3,5-Me$_2$-C$_5$H$_3$N)$_2$Cd(OAc)$_2$] have not been successful. Thus, further applications in cluster synthesis require that (*N*,*N*′-tmeda)Cd(SeSiMe$_3$)$_2$ be generated in situ. The synthesis of ternary derivatives of the adamantoid clusters [M$_{10}$E$_4$(EPh)$_{12}$(L)$_4$] (M = Zn, Cd, Hg) is appealing because the photophysical properties of the corresponding binary derivatives have been described in detail.[16,37−39] Given that these cluster molecules can be structurally characterized, it is possible to establish structure−property relationships regarding the incorporation of a second metal ion within the quantum confinement regime.

$$Cd(OAc)_2 + TMEDA + 2Se(SiMe_3)_2 \rightarrow [(N,N'\text{-tmeda})Cd(SeSiMe_3)_2]\ (\mathbf{1}) \quad (1)$$

The reaction of [(3,5-Me$_2$-C$_5$H$_3$N)$_2$Zn(SeSiMe$_3$)$_2$] with (P^{n}Pr$_3$)$_2$Cd(OAc)$_2$ and PhSeSiMe$_3$ in toluene in a 0.25:1:1.5 ratio produces the cluster [Zn$_{1.8}$Cd$_{8.2}$Se$_4$(SePh)$_{12}$(P^{n}Pr$_3$)$_4$], **2a**, in good yield. An increase in the molar fraction of the zinc (trimethylsilyl)selenolate precursor to 0.35 equiv (with correspondingly less PhSeSiMe$_3$) results in a proportional increase in the Zn content of the cluster, yielding crystals of the cluster compound with stoichiometry [Zn$_{2.6}$Cd$_{7.4}$Se$_4$-(SePh)$_{12}$(P^{n}Pr$_3$)$_4$], **2b** (eq 2). The related ZnCdTe clusters [Zn$_{1.8}$Cd$_{8.2}$Te$_4$(TePh)$_{12}$(P^{n}Pr$_3$)$_4$], **3a**, and [Zn$_{2.6}$Cd$_{7.4}$Te$_4$(TePh)$_{12}$-(P^{n}Pr$_3$)$_4$], **3b**, can be crystallized from similar reactions of [(3,5-Me$_2$-C$_5$H$_3$N)$_2$Zn(TeSiMe$_3$)$_2$] with (P^{n}Pr$_3$)$_2$Cd(OAc)$_2$ and PhTeSiMe$_3$ in toluene (eq 2).

$$X[(3,5\text{-}Me_2\text{-}C_5H_3N)_2Zn(ESiMe_3)_2] + (X+2Y)[(P^nPr_3)_2Cd(OAc)_2] + Y PhESiMe_3 \rightarrow [Zn_xCd_{10-x}E_4(EPh)_{12}(P^nPr_3)_4]\ (\mathbf{2},\mathbf{3})\quad E = Se, Te \quad (2)$$

The structures of clusters **2a** and **3b** were confirmed by X-ray crystallographic analysis (see Table 1). Both clusters crystallize in the tetragonal space group $I4_1/a$ and are crystallographically isomorphous to the binary [Cd$_{10}$Se$_4$-(SePh)$_{12}$(P^{n}Pr$_3$)$_4$][40] and [Zn$_{10}$Te$_4$(TePh)$_{12}$(P^{n}Pr$_3$)$_4$][41] analogues.

(36) Babcock, J. R.; Zehner, R. W.; Sita, L. R. *Chem. Mater.* **1998**, *10*, 2027−2029.
(37) Eichhöfer, A.; Aharoni, A.; Banin, U. *Z. Anorg. Allg. Chem.* **2002**, *628*, 2415−2421.
(38) (a) Eichhöfer, A.; Tröster, E. *Eur. J. Inorg. Chem.* **2002**, 2253−2256. (b) Eichhöfer, A.; Deglmann, P. *Eur. J. Inorg. Chem.* **2004**, 349−355.
(39) Adams, R. D.; Zhang, B.; Murphy, C. J.; Yeung, L. K. *Chem. Commun.* **1999**, 383−384.
(40) Soloviev, V. N.; Eichhöfer, A.; Fenske, D.; Banin, U. *J. Am. Chem. Soc.* **2000**, *122*, 2673−2674.
(41) (a) Eichhöfer, A.; Fenske, D.; Pfistner, H.; Wunder, M. *Z. Anorg. Allg. Chem.* **1998**, *624*, 1909−1914. (b) Pfistner, H.; Fenske, D. *Z. Anorg. Allg. Chem.* **2001**, *627*, 575−582.

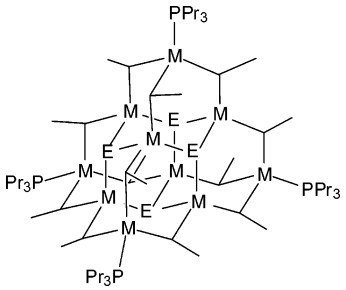

Figure 1. Line diagram representing the fused adamantane structure of the $[M_{10}E_4(EPh)_{12}(P^nPr_3)_4]$ (M = Zn, Cd; M′ = Cd, Hg; E = Se, Te) clusters (**2**−**5**). The site distribution of the metal ions is discussed in the text.

The overall arrangement of metal and chalcogen ions generates a tetrahedral framework consisting of four fused $\{M_4E_6\}$ adamantane units (Figure 1), similar to the building blocks that constitute the cubic (sphalerite) phases of the bulk materials. The four apexes of the tetrahedron are terminated by coordinated phosphine ligands, and this M_{10} architecture is prevalent among II−VI nanoclusters.[37−43] The identities of clusters **2b** and **3a** were verified by determination of the cell constants of single crystals of the compounds.

The metal compositions of all clusters reported herein were determined by EDX analysis on single crystals and confirmed by AAS and elemental analyses.[44] The measured Zn:Cd ratios are remarkably consistent with the amounts incorporated into the reaction scheme, illustrating that the precursor complexes $[(3,5\text{-}Me_2\text{-}C_5H_3N)_2Zn(ESiMe_3)_2]$ are efficient delivery agents of $\{ZnE_2\}$ (E = Se, Te) in cluster synthesis. The inability to fully resolve zinc and cadmium from crystallographic data is indicative of intimate mixing of the metal ions within the clusters. For cluster **3b**, a satisfactory model however was achieved with site occupancy of $Zn_{0.5}Cd_{0.5}$ given to the metal ion sites bonded to the apical P^nPr_3 ligands with the remaining zinc ions distributed among the rest of the core metal sites in the structure. A similar disorder model was attained for the terminal metal sites in cluster **2a** however with a lower Zn occupancy (30%). This leaves $\sim^1/_3$ of the Zn in the cluster to be distributed among the remaining six metal sites in the core of the cluster. This mixing is unlike the positions of the Zn centers in the II−II′−VI nanoclusters $[(N,N'\text{-tmeda})_5Zn_5Cd_{11}E_{13}(EPh)_6]$ in which the chelating *N*,*N*′-tmeda ligands constrain all Zn(II) to the surface the nanoclusters.[27]

A summary of relevant bond distances and angles for clusters **2a** and **3b** is presented in Table 2. The key structural effect of Zn/Cd site disorder at the terminal position in cluster **2a** is observed as a slight deformation of the adamantane cages. The distorted tetrahedral bonding environment of the

Table 2. Selected Interatomic Bond Distances (Å) for Complexes **2a** and **3b**

	$[Zn_{1.8}Cd_{8.2}Se_4(SePh)_{12}(P^nPr_3)_4]$, **2a**		
Cd1−P1	2.572(6)	Cd2−Se1	2.570(1)
Cd1−Se2	2.583(6)	Cd2−Se2	2.705(1)
Cd1−Se3	2.651(5)	Cd2−Se4A	2.696(1)
Cd1−Se4A	2.587(6)	Cd2−Se1A	2.593(1)
Zn1−P1	2.61(2)	Cd3−Se1	2.588(1)
Zn1−Se2	2.685(19)	Cd3−Se1B	2.588(1)
Zn1−Se3	2.459(17)	Cd3−Se3	2.706(1)
Zn1−Se4A	2.65(2)	Cd3−Se3B	2.706(1)
	$[Zn_{2.6}Cd_{7.4}Te_4(TePh)_{12}(P^nPr_3)_4]$, **3b**		
Cd1−P1	2.541(9)	Cd2−Te1	2.738(1)
Cd1−Te2	2.772(8)	Cd2−Te2	2.881(1)
Cd1−Te3A	2.690(8)	Cd2−Te3	2.869(1)
Cd1−Te4B	2.732(9)	Cd2−Te1A	2.762(1)
Zn1−P1	2.543(14)	Cd3−Te1	2.763(1)
Zn1−Te2	2.649(12)	Cd3−Te1B	2.763(1)
Zn1−Te3A	2.796(12)	Cd3−Te4	2.877(1)
Zn1−Te4B	2.748(13)	Cd3−Te4B	2.877(1)

Zn1/Cd1 ion in this position is occupied by one P^nPr_3 and three μ-SePh ligands. The crystallographic structural model indicates that the incorporation of Zn is accommodated primarily by a displacement of the position of the metal center. In this model, the Zn1−Se3 (2.459(17) Å) and Cd1−Se3 (2.651(5) Å) contacts are consistent with the bond distances of the corresponding M1−μ-SePh interactions in $[NEt_4]_2[Zn_8Cl_4Se(SePh)_{12}]$[41a] and $[Cd_{10}Se_4(SePh)_{12}(P^nPr_3)_4]$,[40] respectively. The M1−Se2 and M1−Se4 bond lengths (2.583(6)−2.685(19) Å), on the other hand, lie intermediate between the expected Zn−Se and Cd−Se distances. Interestingly, longer distances are observed for the Zn1−Se than for the Cd1−Se interactions, which are, in turn, shorter than those observed for $[Cd_{10}Se_4(SePh)_{12}(P^nPr_3)_4]$. For their part, the M1−P1 bond distances exhibit a similar effect with short Cd1−P1 and long Zn1−P1 interactions relative to those in related clusters.[41,43]

The Cd atoms present in the cluster center exhibit Cd−μ_4-Se and Cd−μ-SePh interactions that lie within the range of those reported for $[Cd_{10}Se_4(SePh)_{12}(PR_3)_4]$,[40,43] thus favoring an assignment of predominantly Cd to these sites. However, the longest of these contacts in **2a** are significantly shorter than the longest observed in $[Cd_{10}Se_4(SePh)_{12}(PR_3)_4]$, suggesting that a small percentage of zinc exists in the cluster core sites.

The X-ray crystal structure of cluster **3b** shows structural features similar to those of **2a**, with M1−P1 and M1−μ-TePh bond distances that are intermediate between those in the clusters $[Zn_{10}Te_4(TePh)_{12}(P^nPr_3)_4]$[41] (Zn−P = 2.428(4), Zn−Te = 2.630(2)−2.718(1) Å) and $[Cd_{10}Te_4(TePh)_{12}(P^nPr_3)_4]$[37] (Cd−P = 2.618(2), Cd−Te = 2.789(1)−2.898(1) Å). Again, the largest effect is observed in the bond distance of one [M1−Te2] of the M−μ-TePh interactions, which lie within the range of those observed in the binary molecules. The remaining Zn1−μ-TePh bond lengths are comparably longer than the equivalent Cd1−Te distances. For the metal atoms in the cluster core (assigned exclusively to Cd in the structural model), evidence for low levels of Zn is imparted by the average Cd−Te and Cd−TePh bond distances, which are slightly shorter than those reported for $[Cd_{10}Te_4(TePh)_{12}(P^nPr_3)_4]$.[37]

(42) (a) Choy, A.; Craig, D. C.; Dance, I. G.; Scudder, M. L. *Chem. Commun.* **1982**, 1246−1247. (b) Dance, I. G.; Choy, A.; Scudder, M. L. *J. Am. Chem. Soc.* **1984**, *106*, 6285−6295. (c) Nyman, M. D.; Hampden-Smith, M. J.; Duesler, E. N. *Inorg. Chem.* **1996**, *35*, 802−803.

(43) Behrens, S.; Bettenhausen, M.; Eichhöfer, A.; Fenske, D. *Angew. Chem., Int. Ed. Engl.* **1997**, *36*, 2797−2798.

(44) While EDX analysis provides only semiquantitative elemental analysis, the reliability of these data regarding the metal ion composition of the clusters was confirmed by quantitative measurement of the Zn/Cd content of clusters **1a** and **2b** using atomic absorption spectroscopy.

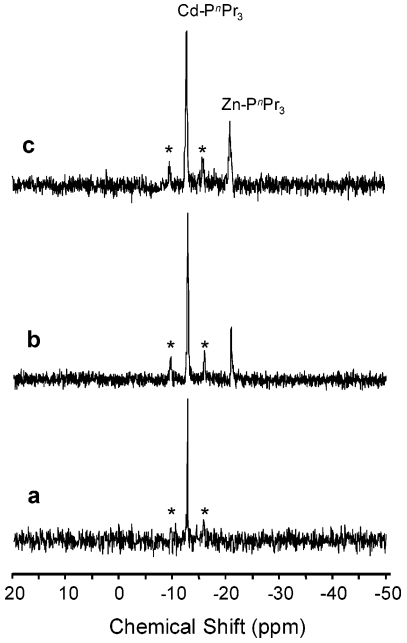

Figure 2. $^{31}P\{^1H\}$ NMR spectra of (a) $[Cd_{10}Se_4(SePh)_{12}(P^nPr_3)_4]$, (b) cluster **2a**, and (c) cluster **2b** in CD_2Cl_2. $^{111}Cd/^{113}Cd$ satellites are denoted with asterisks.

Further support for the assignment of Zn(II) at the peripheral sites was provided by $^{31}P\{^1H\}$ NMR spectroscopy (Figure 2). The $^{31}P\{^1H\}$ NMR spectrum of the CdSe cluster $[Cd_{10}Se_4(SePh)_{12}(P^nPr_3)_4]$ (Figure 2a) shows a broad (fwhm = 21.3 Hz) single resonance at −12.8 ppm. The single peak is consistent with the chemical equivalence of the four phosphine ligands on the cluster, and the downfield shift relative to that of free P^nPr_3 (−32.0 ppm) corresponds with the effect observed in phosphine-coordinated cadmium complexes.[45] For clusters **2a,b** a second peak at −21.1 ppm is observed in the $^{31}P\{^1H\}$ NMR spectra in addition to that assigned to a Cd−P interaction (Figure 2b,c). Consistent with the effect observed in coordination complexes of zinc and cadmium,[45] this peak can be attributed to a Zn−P interaction. The relative ratios of Zn:Cd at these sites are qualitatively comparable to those determined by X-ray crystallography (i.e. **2a**, 30:70). In all cases, the Cd−P resonances were accompanied by satellites due to $^{113}Cd-^{31}P$ and $^{111}Cd-^{31}P$ coupling. The Cd−P coupling constants [$^1J(^{113}Cd-^{31}P)$ = 497 Hz; $^1J(^{111}Cd-^{31}P)$ = 530 Hz] are significantly smaller than those reported for mononuclear cadmium phosphine complexes,[46,47] indicating that the Cd−P interactions are weaker in the cluster compounds. $^{31}P\{^1H\}$ NMR spectroscopic data for clusters **3a**,**b** were consistent with the estimated Zn:Cd ratio at the terminal positions, with two peaks of similar intensity observed at −20.9 and −25.4 corresponding to Cd−P and Zn−P interactions, respectively.

The considerable fraction of the Zn ions being located at the apical sites in these clusters is interesting because it is inconsistent with the expected positions on the basis of the integration of preformed $\{ZnE_2\}$ units in the synthetic scheme. At the apical positions, metal centers are bonded only to a phosphine ligand and three bridging $PhSe^-$ ligands. Thus, it would be anticipated that these sites would contain a low percentage of Zn because the Zn−E interactions present in the precursor complexes $[(3,5\text{-}Me_2\text{-}C_5H_3N)_2Zn(ESiMe_3)_2]$ must be broken to accommodate this transfer. Notable in this discussion is the observed retention of the $\{(N,N'\text{-tmeda})ZnE_2\}$ units in the structures of $[(N,N'\text{-tmeda})_5Zn_5Cd_{11}E_{13}(EPh)_6]$.[27] Thus, it is rather unlikely that the solution decomposition of the precursor to form $E(SiMe_3)_2$ preceded the reaction of the complexes with $Cd(OAc)_2$, especially in the case of the selenolate analogue, which is stable for short periods even at 0 °C. For the Te complexes, the addition of $[(3,5\text{-}Me_2\text{-}C_5H_3N)_2Zn(TeSiMe_3)_2]$ to the $Cd(OAc)_2$ solution at −78 °C results in an abrupt color change, suggesting the formation of Zn−Te−Cd interactions ($[(3,5\text{-}Me_2\text{-}C_5H_3N)_2Zn(TeSiMe_3)_2]$ is stable for extended periods in solution at this temperature). As the temperature is increased, Zn−E bond cleavage must result in a "migration" of the zinc to the peripheral sites. The preferential occupation of zinc at these positions (versus core sites) may then be attributed to an increased flexibility in bonding arrangement and distances at the exterior of the clusters relative to those in the cluster core.

In addition to the effects of Zn incorporation on the optical properties of the clusters (vide infra), the presence of Zn ions at the terminal positions appears to have a marked effect on the relative stability of the cluster complexes. This is evidenced by the fact that clusters **2a,b** can be stored for extended periods in THF. In contrast, it has been reported[40] that the dissolution of $[Cd_{10}Se_4(SePh)_{12}(PPh_3)_4]$ in THF leads to the formation of $[Cd_{32}Se_{14}(SePh)_{36}(PPh_3)_4]$ within a few days. Thus, the synthesis of binary $\{Cd_{10}Se\}$ clusters is typically carried out in DME or toluene.[37] The ternary ZnCdTe analogues, **3a**,**b**, similarly show an increased stability in the solid state. Crystalline samples of these clusters remain unchanged for weeks at room temperature under inert atmosphere, whereas the complex $[Cd_{10}Te_4(TePh)_{12}(PPh_3)_4]$ decomposes to an optically and spectroscopically different compound under the same conditions.[48]

The use of metal (trimethylsilyl)chalcogenolate complexes can readily be applied to the synthesis of ternary ZnHgSe and CdHgSe clusters. Reaction of complex $[(3,5\text{-}Me_2\text{-}C_5H_3N)_2Zn(SeSiMe_3)_2]$ with $(P^nPr_3)_2HgCl_2$ in the presence of $PhSeSiMe_3$ in toluene generates the cluster $[Zn_3Hg_7Se_4(SePh)_{12}(P^nPr_3)_4]$, **4** (eq 3). If $[(3,5\text{-}Me_2\text{-}C_5H_3N)_2Zn(SeSiMe_3)_2]$ is substituted with $(N,N'\text{-tmeda})Cd(SeSiMe_3)_2$, then single crystals of $[Cd_{3.7}Hg_{6.3}Se_4(SePh)_{12}(P^nPr_3)_4]$, **5**, can be isolated in low yield (eq 4). Again, the metal ion stoichiometry was determined by EDX and elemental analysis on single crystals of the cluster compounds.[44] The disparity between the metal content in cluster **5** and the observed Cd/Hg ratio is interesting; however, the low yield of this complex precludes any rationalization in terms of the

(45) Kessler, J. M.; Reeder, J. H.; Vac, R.; Yeung, C.; Nelson, J. H.; Frye, J. S.; Alcock, N. W. *Magn. Reson. Chem.* **1991**, *29*, S94−105.
(46) Goel, R. G.; Henry, W. P.; Jha, N. K. *Inorg. Chem.* **1982**, *21*, 2551−2555.
(47) (a) Mann, B. E. *Inorg. Nucl. Chem. Lett.* **1971**, *7*, 595−597. (b) Meehan, P. R.; Ferguson, G.; Shakya, R. P.; Alyea, E. C. *J. Chem. Soc., Dalton Trans.* **1997**, 3487−3491.
(48) Eichhöfer, A. Personal communication.

Table 3. Selected Interatomic Bond Distances (Å) and Angles (deg) for Complex **5**

Hg1−P1	2.496(8)	P1−Hg1−Se2	111.05(6)
Hg1−Se2	2.649(2)	Se3−Hg2−Se2	90.41(17)
Hg2−Se3	2.531(8)	Se3−Cd2−Se2	91.53(10)
Hg2−Se2	2.801(13)	Hg1−Se2−Cd2	104.3(2)
Cd2−Se3	2.609(7)	Hg1−Se2−Hg2	101.5(3)
Cd2−Se2	2.678(9)	C35−Se2−Cd2	106.6(6)

increased stability associated with the higher Cd content.

$$0.35[(3,5\text{-}Me_2\text{-}C_5H_3N)_2Zn(SeSiMe_3)_2] + [(P^nPr_3)_2HgCl_2] + 1.3PhSeSiMe_3 \rightarrow [Zn_3Hg_7Se_4(SePh)_{12}(P^nPr_3)_4]\ (\mathbf{4}) \quad (3)$$

$$0.35[(N,N'\text{-tmeda})Cd(SeSiMe_3)_2]\ (\mathbf{1}) + [(P^nPr_3)_2HgCl_2] + 1.3PhSeSiMe_3 \rightarrow [Cd_{3.7}Hg_{6.3}Se_4(SePh)_{12}(P^nPr_3)_4]\ (\mathbf{5}) \quad (4)$$

Clusters **4** and **5** crystallize in the cubic space groups $I\bar{4}3m$ and $F\bar{4}3c$, respectively. Similar to clusters **2** and **3**, as well as recently reported binary HgSe clusters,[38] the structures exhibit the well-known fused tetraadamantane cage architecture (Figure 1) that also comprises the extended structure of bulk cubic HgSe. For cluster **5**, the phenyl groups and carbon atoms of the phosphine ligands are disordered over two positions with equal occupancy. In the case of complex **4**, the structure was solved as two independent molecules. The inability to resolve Zn in the molecules is attributable to the relatively weak diffraction data and small crystal size; however, substantially larger thermal parameters for the six core metal positions compared to the terminal sites suggest that the Zn ions occupy these (disordered) positions. UV−vis data also indicate interstitial locations for the Zn(II) (vide infra). For the Cd−Hg−Se cluster **5**, the crystallographic model refined most suitably with a 0.7:0.3 Cd/Hg disorder assigned to the six core metal positions. No cadmium was assigned to the four apical metal ion sites. The molecular formula $[Cd_{4.2}Hg_{5.8}Se_4(SePh)_{12}(P^nPr_3)_4]$ obtained from crystallographic refinement is in near agreement with the $\{Cd_{3.7}Hg_{6.3}\}$ stoichiometry determined by EDX analyses. Examination of the bond distance data for cluster **5** (Table 3) further supports the assignment of the metal positions discussed above. The Hg−μ-SePh and Hg−P1 bond distances are similar to those in other binary HgSe clusters[38a,49] suggesting predominantly Hg at the apical positions. The concentration of the lighter metal ion within the cores of clusters **4** and **5** contrasts with the metal ion distributions determined for the ZnCdSe and ZnCdTe complexes **2** and **3**, in which the zinc centers preferentially occupy peripheral sites in the cluster. In view of the discussion above, this may be a result of the low-temperature synthesis of the Hg-containing clusters, such that the cleavage of Zn−Se and Cd−Se bonds in the polynuclear framework may be inhibited. Alternatively, this arrangement may again reflect the site preference of the individual metal atoms. The prevalence of the larger (Hg) metal ion at the terminal sites is contrary to that observed for clusters **2** and **3**. This can be explained by the relative lability of the P^nPr_3 versus −SePh ligands and the propensity of Hg over Zn and Cd to adopt lower coordination geometries.[50] In metal chalcogen cluster complexes containing mercury, linear or trigonal coordination of the Hg centers has been observed.[24,51] In a most related case, the solid-state structure of the fused adamantoid/barrelanoid cluster $[Hg_{32}Se_{14}(SePh)_{36}]$ consists of Hg(II) ions at the terminal positions that are coordinated only to three −SePh ligands in distorted trigonal planar fashion.[38a,52] Even if phosphine ligands are provided in the synthetic scheme,[38a] the cluster crystallizes with "uncapped" Hg centers at the cluster terminus. In relation to clusters **4** and **5**, the presence of largely Hg ions at the peripheral sites may be due to an increased ability to accommodate phosphine exchange in solution.

Repeated efforts to prepare the sulfur analogues of clusters **2** and **3**, $[Zn_xCd_{10-x}S_4(SPh)_{12}(P^nPr_3)_4]$, via the reaction of $[(3,5\text{-}Me_2\text{-}C_5H_3N)_2Zn(SSiMe_3)_2]$ with $Cd(OAc)_2$ or $CdCl_2$ were unsuccessful. Instead, these reactions invariably led to the isolation of the larger ternary cluster $[Zn_{2.3}Cd_{14.7}S_4(SPh)_{26}(P^nPr_3)_2]$, **6** (eq 5). The inability to isolate the corresponding M_{10} derivative was rather surprising considering the well-documented stability of the $[M_{10}S_4(SPh)_{16}]^{4-}$.[42] The formation of these and other polynuclear metal−sulfur complexes cannot be precluded, however, in view of the relatively low yield and zinc deficiency (with respect to the reaction stoichiometry) of cluster **6**.

$$0.28[(3,5\text{-}Me_2\text{-}C_5H_3N)_2Zn(SSiMe_3)_2] + [(P^nPr_3)_2Cd(OAc)_2] + 1.4PhSSiMe_3 \rightarrow [Zn_{2.3}Cd_{14.7}S_4(SPh)_{26}(P^nPr_3)_2]\ (\mathbf{6}) \quad (5)$$

The structure of cluster **6** was solved and refined (Table 1) in the space group $I2$ with two chemically equivalent but crystallographically independent molecules in the asymmetric unit. The supertetrahedral $[M_{17}S_{28}]^{2+}$ core of the cluster consists of four edge- and vertex-sharing adamantane cages with terminating barrelanoid cages residing at the four corners of the tetrahedron (Figure 3). The latter are representative of the fundamental structural unit of the hexagonal (*wurtzite*) CdS system. Either P^nPr_3 or −SPh ligands occupy the terminal coordination sites on the four apical metal centers. The cluster architecture is analogous to those of the previously reported cluster $\{[Cd_{17}S_4(SPh)_{28}]^{2-}\}$[53] as well as the selenium derivative $\{[Cd_{17}Se_4(SePh)_{24}(PPh_3)_4]^{2+}\}$.[54] The combination of two neutral P^nPr_3 and two anionic PhS^- ligands at the terminal positions of the structure leads to the overall neutral charge of cluster **6**, which represents the first discrete neutral group XII M_{17} cluster. The cluster solid $[Cd_{17}S_4(SCH_2CH_2OH)_{26}]$ is also charge neutral; however, this

(49) Behrens, S.; Fenske, D. *Ber. Bunsen-Ges. Phys. Chem.* **1997**, *101*, 1588−1592.
(50) Kaupp, M.; von Schnering, H. G. *Inorg. Chem.* **1994**, *33*, 2555−2564.
(51) Bettenhausen, M.; Fenske, D. *Z. Anorg. Allg. Chem.* **1998**, *624*, 1245−1246.
(52) Fenske, D.; Bettenhausen, M. *Angew. Chem., Int. Ed.* **1998**, *37*, 1291−1294.
(53) Lee, G. S. H.; Craig, D. C.; Ma, I.; Scudder, M. L.; Bailey, T. D.; Dance, I. G. *J. Am. Chem. Soc.* **1988**, *110*, 4863−4864.
(54) Behrens, S.; Bettenhausen, M.; Deveson, A. C.; Eichhöfer, A.; Fenske, D.; Lohde, A.; Woggon, U. *Angew. Chem. Int. Ed. Engl.* **1996**, *35*, 2215−2218.

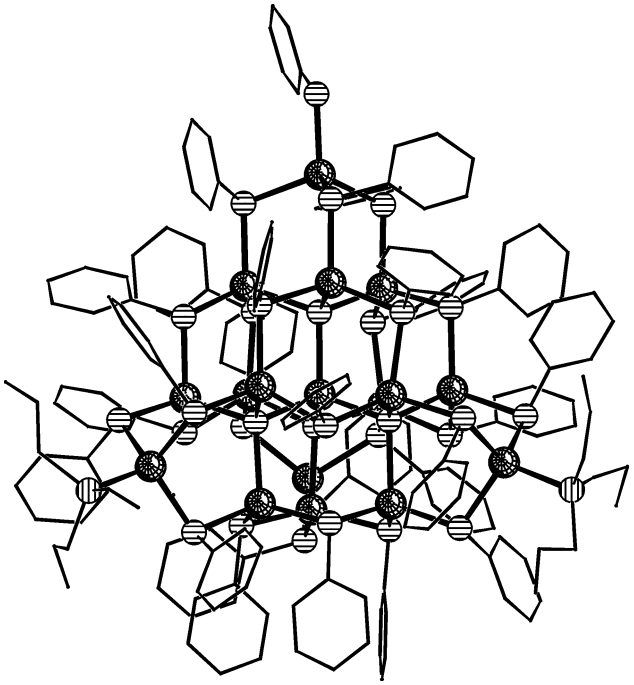

Figure 3. Ball and stick representation of the molecular structure of cluster **6**. For clarity, the carbon atoms of the −SPh and P^nPr_3 ligands are shown as lines (H atoms omitted). Relevant bond distances (Å): Cd−μ_4-S = 2.45(4)−2.58(4), Cd−μ-SPh = 2.47(4)−2.60(4), Cd−SPh = 2.46(5)−2.47(5), Cd−P = 2.50(8)−2.57(8).

is achieved via bridging interactions of the terminal thiolates between cluster units resulting in a lattice network.[55] Crystallographic data did not afford unambiguous assignment of Zn(II) to any of the metal ion positions in cluster **6**, and a satisfactory model was attained with cadmium assigned to all metal sites. Nonetheless, the presence of zinc(II) within the cluster was verified reproducibly by EDX analysis on single crystals, which revealed a 6.4:1 (Cd:Zn) stoichiometry, yielding an average composition of $Zn_{2.3}Cd_{14.7}$ for the cluster molecules.[44] Although weak diffraction data precluded an explicit assignment of zinc(II) to any of the metal sites on the basis of atomic thermal parameters or bond distance data, derivative evidence for the presence of zinc(II) at the apical positions of the cluster was provided again by $^{31}P\{^1H\}$ NMR spectroscopy. The $^{31}P\{^1H\}$ NMR spectrum of this complex reveals two shifts at −5.6 and −13.1 ppm and can be assigned to Cd−P^nPr_3 and Zn−P^nPr_3 interactions, respectively.

Optical Properties of the Ternary II−II′-VI Clusters. The low-temperature absorption spectra of clusters **2a,b** are presented in Figure 4, together with that of the analogous binary $[Cd_{10}Se_4(SePh)_{12}(P^nPr_3)_4]$.[16] Within the series, a modest yet discernible shift to higher energy of the absorption onset is observed with increasing Zn content. A corresponding blue shift in the absorption maximum of the first transition occurs with experimental values of 302, 310, and 321 nm obtained for clusters **2a**, **2b**, and $[Cd_{10}Se_4(SePh)_{12}(P^nPr_3)_4]$, respectively. Consistent with the assignment of this absorption to the first "excitonic" transition in other $\{M_{10}\}$

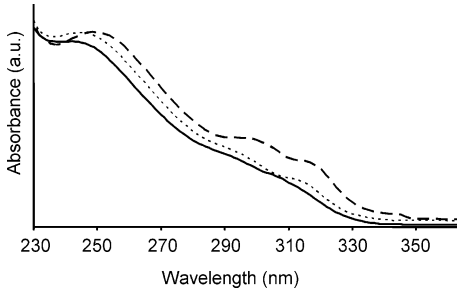

Figure 4. Absorption spectra of $[Cd_{10}Se_4(SePh)_{12}(P^nPr_3)_4]$ (− − −), $[Zn_{1.8}Cd_{8.2}Se_4(SePh)_{12}(P^nPr_3)_4]$, **2a** (---), and $[Zn_{2.6}Cd_{7.4}Se_4(SePh)_{12}(P^nPr_3)_4]$, **2b** (—) measured at 200 K in CH_2Cl_2. The data are normalized for comparison.

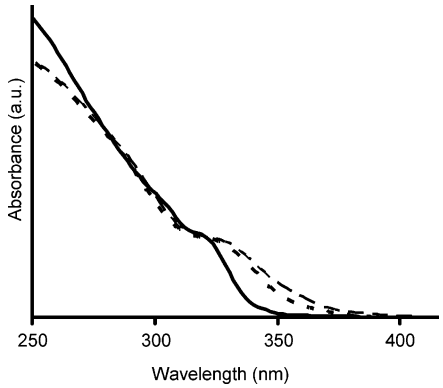

Figure 5. Absorption spectra of $[Zn_{1.8}Cd_{8.2}Te_4(TePh)_{12}(P^nPr_3)_4]$, **2a**, $[Zn_{2.6}Cd_{7.4}Te_4(TePh)_{12}(P^nPr_3)_4]$, **3b**, and $[Cd_{10}Te_4(TePh)_{12}(P^nPr_3)_4]$ measured at 200 K in CH_2Cl_2. The data are normalized for comparison.

cluster molecules,[16,37] these results correspond to effective "band gap" energies that can be tuned from 4.1 to 3.86 eV. These effects are in concert with the relative band gap energies of ZnSe (2.6 eV) and CdSe (1.7 eV) semiconductor solids, as well as the trend reported for $Zn_xCd_{1-x}Se$ nanoparticles.[13] Although the spectra of **2a**,**b** were obtained on single-crystalline samples of the clusters, the absorption profiles are somewhat broader than those of the binary Cd_{10} derivatives (Figure 4). The stoichiometry of the ternary clusters indicates that they requisitely contain a mixture of species [i.e. (Zn_2Cd_8), (Zn_3Cd_7)], accounting for this effect. Although a statistical distribution of Zn(II) [i.e. Zn_0:Zn_{10}] in the individual clusters is possible, this is not supported by the shapes of the absorption profiles. Clearly, no absorption maxima are assignable to the all cadmium cluster $[Cd_{10}Se_4(SePh)_{12}(P^nPr_3)_4]$.[16] This is consistent with previous reports, demonstrated via electrospray mass spectrometric and NMR analysis, for selective Zn:Cd ratios in mixed-metal M_{10} and M_{17} sulfide/thiolate nanoclusters.[56]

A similar pattern is observed for the series $[Zn_xCd_{10-x}Te_4(TePh)_{12}(P^nPr_3)_4]$ (Figure 5) with "excitonic" maxima ranging from 321 nm (3.86 eV) to 328 nm (3.78 eV). Clusters **2** and **3** are luminescent only at low temperature, featuring broad emission maxima that are significantly shifted to lower energy relative to the excitation onset (see Supporting Information). Consistent with the optical properties of related

(55) Vossmeyer, T.; Reck, G.; Katsikas, L.; Haupt, E. T. K.; Schulz, B.; Weller, H. *Science* **1995**, *267*, 1476−1479.

(56) (a) Løver. T.; Henderson, W.; Bowmaker, G. A.; Seakins, J. M.; Cooney, R. P. *Inorg. Chem.* **1997**, *36*, 3711−3723. (b) Dance, I. G. *Aust. J. Chem.* **1985**, *38*, 1745−1755.

CdSe and CdTe clusters, the "trapped" emission is assigned to forbidden transitions involving the surface phenylchalcogenolate ligands.[16,37] Since the luminescence in these clusters arises from ligand-based transitions, the presence of Zn(II) in the cluster is not expected to affect the photoluminescence. Indeed, the emission energy of cluster **2** is identical with that of the binary $[Cd_{10}Se_4(SePh)_{12}(P^nPr_3)_4]$ cluster.

The observed effects in the optical spectra can be rationalized in the following manner: considering the constitution of the valence and conduction bands in bulk CdSe and CdTe, the lowest energy band in the absorption spectra of $[Cd_{10}E_4(EPh)_{12}(P^nPr_3)_4]$ (E = Se, Te) is expected to arise from a 4p (Se^{2-})/5p (Te^{2-}) → 5s (Cd^{2+}) transition. The introduction of Zn^{2+} introduces orbitals in the form of 4s (Zn^{2+}). If we consider the clusters $[Zn_xCd_{10-x}E_4(EPh)_{12}(P^nPr_3)_4]$ (**2**, **3**) to be molecular species with truly discrete bonding and antibonding orbitals, the position of the first absorption should not change upon the incorporation of Zn^{2+} because the energy of the lowest unoccupied molecular orbital (LUMO) would not change. Thus, the effects of Zn^{2+} incorporation would involve merely a decrease in the intensity of the first transition observed in the all cadmium derivative and the coincident appearance of a higher energy band corresponding to a 4p (Se^{2-})/5p (Te^{2-}) → 4s (Zn^{2+}) transition. The observed blue shift of the absorption in clusters **2a,b** supports previous accounts[16] associating the optical properties of CdSe clusters with those of nanocrystalline compounds. The optical spectra of the ZnCdE clusters **2** and **3** are consistent with this analogy and suggest the mixing of orbitals resulting in a "pseudoband" structure. Thus, $[Zn_xCd_{10-x}E_4(EPh)_{12}(P^nPr_3)_4]$ (E = Se, Te) can be viewed as molecular models of ternary $Zn_xCd_{10-x}E$ nanoparticles and semiconductor solids.

The moderate shift to higher energy of the first absorption upon the incorporation of Zn in clusters **2** and **3** is consistent with the prevalence of Zn(II) in the terminal positions of the tetraadamantane cages where there are no Zn−(Se^{2-}/Te^{2-}) bonding interactions. Thus, the position of the lowest energy transition should be more strongly influenced by the zinc ions that occupy the six core sites versus those at the cluster periphery. This accounts for the modest differences in the absorption onset for the $[Zn_xCd_{10-x}E_4(EPh)_{12}(P^nPr_3)_4]$ clusters **2** and **3** versus the binary CdE analogues.

The instability of the ternary MHgSe clusters in solution required that their optical properties be examined in the solid state. The diffuse reflectance UV−visible spectra of clusters **4** and **5** are displayed in Figure 6. The spectrum of cluster **4** exhibits an absorption shoulder at 370 nm (3.35 eV) that is significantly shifted to higher energy relative to that of the binary cluster $[Hg_{10}Se_4(SePh)_{12}(PPh_2{}^nPr)_4]$ (410 nm, 3.02 eV).[38a] Cluster **5** exhibits a similar absorption profile but with the excitonic absorption maximum observed at slightly higher energy (364 nm, 3.40 eV). Although the observation of a higher energy transition in the spectrum of **5** versus that of **4** contrasts with the relative band gap energies of ZnSe and CdSe, the effect can easily be rationalized by the higher M′ content in the former. More interesting is that the shifts in the absorption spectra of complexes **4** and **5** (relative to that of the binary HgSe analogue) are substantially greater than

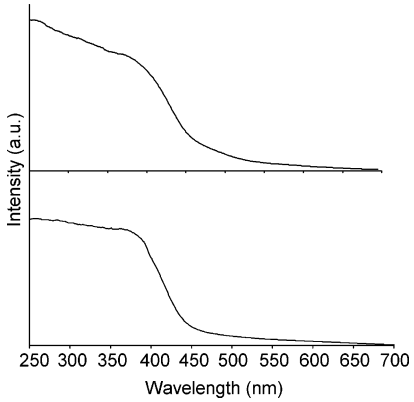

Figure 6. Room-temperature diffuse reflectance UV−visible spectrum of $[Zn_3Hg_7Se_4(SePh)_{12}(P^nPr_3)_4]$, **4**, and $[Cd_{3.7}Hg_{6.3}Se_4(SePh)_{12}(P^nPr_3)_4]$, **5**, diluted in KBr.

observed with Zn(II) incorporation in the ZnCdSe system (vide supra). These outcomes support the notion that the optical properties of these ternary compounds are dictated primarily by the identity of the core metal ions and the assignment of the lowest energy band in the absorption spectra to a Se^{2-}−M transition.

Solid-State Thermolysis of the Clusters. The accessibility, stability, and ease of handling exhibited by metal chalcogen clusters have generated interest in the use of these complexes as precursors to larger compounds.[57−59] The discrete, "premixed" nature of these cluster molecules, combined with their labile ancillary ligands, may afford alternate, low-temperature routes into corresponding (and possibly new) solid-state materials.

Thermogravimetric analysis of complexes **2a**,**b** under inert-atmosphere conditions showed that the thermolytic pathway for cluster degradation involves two successive steps (Figure 7). SDTA reveals one process occurring in the first step (180−260 °C), while three distinct peaks can be observed in the latter stage (290−420 °C). The experimental weight losses associated with the first step for both clusters (**2a**, 15.4%; **2b**, 15.9%) are consistent with the theoretical values (16.5% and 16.7%, respectively) corresponding to the complete removal of the four terminal phosphine ligands. Concurrent transfer of the TGA purge gas to a GC/MS instrument confirmed P^nPr_3 as the primary constituent during this stage. Interestingly, there exists a modest shift in the peak position of the SDTA curve to higher temperature for cluster **2b** (240 °C) versus **2a** (235 °C). The origin of this effect can perhaps be attributed to the relative strengths of Zn−P and Cd−P consistent with the apparent higher ratio of Zn in the terminal phosphine-bound positions of cluster **2b** (vide supra).

The second segment of the cluster decomposition pathway corresponds to the loss of the −SePh ligands via the

(57) (a) Cumberland, S. L.; Hanif, K. L.; Javier, A.; Khitrov, G. A.; Strouse, G. F.; Woessner, S. M.; Yun, C. S. *Chem. Mater.* **2002**, *14*, 1576−1584. (b) Osterloh, F. E.; Hewitt, D. P. *Chem. Commun.* **2003**, 1700−1701.

(58) (a) Eichhöfer, A.; Beckmann, D.; Fenske, D.; Herein, H.; Krautscheid, H. *Isr. J. Chem.* **2001**, *41*, 31−37. (b) Eichhöfer, A.; Fenske, D.; Scheer, P. *Eur. J. Inorg. Chem.* **2004**, 93−97.

(59) Kowalchuk, C.; Corrigan, J. F.; Huang, Y. *Chem. Commun.* **2000**, 1811−1812.

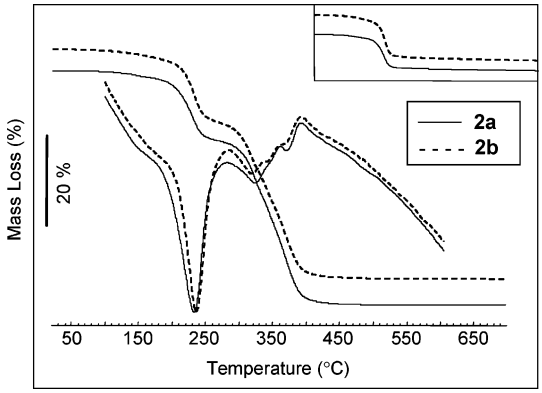

Figure 7. TGA and SDTA curves for the solid-state thermolysis of clusters **2a** (—) and **2b** (---). The inset shows the single weight loss observed in the TGA curves of the resulting solids obtained after heating the clusters to 250 °C and holding at that temperature.

generation and elimination of 6 equiv of Ph_2Se (**2a**, expt 36.8%, calcd 36.2%; **2b**, expt 35.2%, calcd 36.5%). The identity of this product was also confirmed by GC/MS. The loss of Ph_2Se can be paralleled with the formation of six Se^{2-} ligands via Se−C bond homolysis. Powder X-ray diffraction analysis of the corresponding black crystalline solids revealed that these products are phase pure ternary $Zn_xCd_{1-x}Se$ with the hexagonal (*wurtzite*) lattice structure. The composition and uniform distribution of metal ions in these materials were determined using the linear dependency of cell constants on the stoichiometry of alloyed compounds (Vegard's law).[60] The calculated lattice parameters correspond to stoichiometries of $Zn_{0.20}Cd_{0.80}Se$ and $Zn_{0.25}Cd_{0.75}Se$, respectively, consistent with those of the cluster precursors.

The TGA curves of clusters **3a**,**b** show a similar two-step decomposition pathway as observed for complexes **2a,b**, with the loss of the four terminal phosphine ligands (**2a**, expt 13.3%, calcd 13.8%; **2b**, expt 13.0%, calcd 13.9%) preceding the generation and elimination of $TePh_2$ (**3a**, expt 35.0%, calcd 36.5%; **3b**, expt 35.8%, calcd 36.7%) (eq 6). The residual crystalline products were found to be cubic $Zn_{0.15}Cd_{0.85}Te$ and $Zn_{0.24}Cd_{0.76}Te$ by powder X-ray diffraction.

$$[Zn_xCd_{10-x}E_4(EPh)_{12}(P^nPr_3)_4] \rightarrow 10Zn_xCd_{1-x}E + 4P^nPr_3 + 6\,Ph_2E \quad E = Se, Te \quad (6)$$

The segmented nature of the thermolysis of clusters **2** and **3** provided an opportunity to further investigate the process of decomposition for these complexes. If the temperature is maintained following the complete removal of phosphine ligands for **2a,b** (250 °C), no further weight loss occurs (see Figure 7 inset), indicating that the removal of phosphine results in the formation of a metastable species with a composition $[Zn_xCd_{10-x}E_4(EPh)_{12}]$. Farneth et al. reported similar results for the thermolysis of $[(NMe_4)]_4[Cd_{10}S_4(SPh)_{16}]$, with the isolation of an intermediate species with a composition $[Cd_{10}S_4(SPh)_{12}]$.[61] The intermediate was postulated to occur via the attack of the terminal −SPh groups on the tetraalkylammonium cations producing a (NMe_4SPh) side product. The authors suggested that the intermediate consisted of aggregated, but intact, $\{Cd_{10}\}$ cluster units; however, this seems rather unlikely considering marked red shift in the excitation maximum of the intermediate species (400 nm) versus that of the CdS cluster precursor (290−300 nm). Indeed, similar thermal treatment of $[Cd_{10}Se_4(SePh)_{12}(PR_3)_4]$ has been shown to result in the formation of $[Cd_{32}Se_{14}(SePh)_{36}(thf)_4]$ following crystallization from THF solution.[62] The complete elimination of phosphine ligands during thermolysis was confirmed by ^1H and $^{31}P\{^1H\}$ NMR spectroscopy, and only resonances associated with the phenylselenolate ligands were observed in the ^1H NMR spectra. The bright yellow (**7a,b** from **2a,b**) and orange (**8a,b** from **3a,b**) products isolated after such treatments are soluble in polar solvents such as THF or DMF. The solution absorption spectra of these complexes (see Supporting Information) showed a marked red-shift of the lowest energy transition relative to those of the $\{M_{10}\}$ precursors, suggesting the formation of larger cluster compounds. Bright yellow single crystals of **7a,b** have been isolated by slow concentration of solutions in THF; however, these were not suitable for X-ray analysis. While the identity of these compounds has not been confirmed structurally, elemental analysis data are consistent with the equivalent formation of ternary Zn/Cd derivatives of the expanded tetrahedral $\{Cd_{32}Se\}$ cluster. The absorption maxima in the spectra of **7a,b** are shifted to higher energy versus that reported for $[Cd_{32}Se_{14}(SePh)_{36}(PPh_3)_4]$,[16] consistent with the results observed for clusters **2a,b**; however, this shift in λ_{max} is substantially greater than the shift observed for the latter. This implies a greater concentration of Zn(II) ions in the core positions of **7** relative to the $\{M_{10}\}$ complexes. Further support for the formation of larger cluster derivatives is provided by the PXRD patterns of **7a**,**b**, which are similar to that of the binary $Cd_{32}Se$ cluster,[16] however, with peak positions shifted slightly to larger angles. Furthermore, dynamic light scattering experiments revealed particle sizes in the 2.8−2.9 nm range for clusters **7a**,**b**, and this can be compared to the size (3.1 nm) obtained for $[Cd_{32}Se_{14}(SePh)_{36}(PPh_3)_4]$ from similar experiments.[63] Size analysis experiments on solutions of **8a**,**b** revealed that these particles are substantially larger, suggesting that the analogous $M_{32}Te$ cluster is not obtained in these thermodegradation reactions. The PXRD patterns of these compounds can be indexed to the cubic modification. The metal ion ratios $[Zn_{0.17}Cd_{0.83}]$ (**7a**), $[Zn_{0.27}Cd_{0.73}]$ (**7b**), $[Zn_{0.19}Cd_{0.81}]$ (**8a**), and $[Zn_{0.25}Cd_{0.75}]$ (**8b**) were determined by EDX analysis and are consistent with those present in the precursor clusters.

(60) Vegard, L. *Z. Phys.* **1921**, *5*, 17−26.

(61) Farneth, W. E.; Herron, N.; Wang, Y. *Chem. Mater.* **1992**, *4*, 916−922.

(62) Eichhöfer, A. Personal communication.

(63) Eichhöfer, A.; von Hänisch, C.; Jacobsohn, M.; Banin, U. *Mater. Res. Symp. Proc.* **2001**, *636*, D9.53−63.

Conclusions

The use of the silylated zinc(II) and cadmium(II) chalcogenolate complexes reported here offers a general route for the controlled and efficient introduction of Zn or Cd in ternary nanocluster and colloidal synthesis. The synthesis of a series of $[M'_xM_{10-x}E_4(EPh)_{12}(P^nPr_3)_4]$ (M, M′ = Zn, Cd, Hg; E = Se, Te) cluster complexes with similar structures afforded the opportunity to examine the effects of M′ incorporation on the photophysical properties of these molecules. It was observed that the absorption spectra of these nanoclusters could be modulated by controlling the metal ion composition and that the distribution of metal ions within the cluster framework had a marked effect on the stability of the cluster as well as the optical properties. Furthermore, solid-state thermolysis of the ZnCdSe and ZnCdTe complexes revealed that these clusters are single-source precursors not only to bulk ternary $Zn_xCd_{1-x}Se$ and $Zn_xCd_{1-x}Te$ materials but also larger intermediate clusters that can be isolated under mild conditions. The metal ion ratios present in the cluster precursors are retained in the thermolysis products.

Note added in proof: Full details on the thermally induced condensation of CdSe clusters were reported during the revision stage of this manuscript. See Eichhöfer, A. *Eur. J. Inorg. Chem.* **2005**, *7*, 1245−1253.

Acknowledgment. We gratefully acknowledge the Natural Sciences and Engineering Research Council (NSERC) of Canada and the Government of Ontario's PREA program for financial support of this research. We thank Prof. P. D. Harvey (Université de Sherbrooke) for his assistance with the PL and PLE measurements. Dr. A. Eichhöfer (Institüt für Nanotechnologie, Karlsruhe, Germany) is thanked for providing samples of $[Cd_{10}Se_4(SePh)_{12}(P^nPr_3)_4]$ and $[Cd_{10}Te_4(TePh)_{12}(P^nPr_3)_4]$. The Canada Foundation for Innovation, NSERC, and The University of Western Ontario are also acknowledged for equipment funding. M.W.D. thanks the NSERC for a postgraduate scholarship.

Supporting Information Available: X-ray crystallographic files in CIF format for clusters $[Zn_{1.8}Cd_{8.2}Se_4(SePh)_{12}(P^nPr_3)_4]$ (**2a**), $[Zn_{2.6}Cd_{7.4}Te_4(TePh)_{12}(P^nPr_3)_4]$ (**3b**), $[Zn_3Hg_7Se_4(SePh)_{12}(P^nPr_3)_4]$ (**4**), $[Cd_{3.7}Hg_{6.3}Se_4(SePh)_{12}(P^nPr_3)_4]$ (**5**), and $[Zn_{2.3}Cd_{14.7}S_4(SPh)_{26}(P^nPr_3)_2]$ (**6**), crystallographic disorder models, NMR spectra for the precursor complex [(*N*,*N*′-tmeda)Cd(SeSiMe$_3$)$_2$] (**1**), a $^{31}P\{^1H\}$ NMR spectrum for complex **3b**, TGA/SDTA curves for the thermolysis of clusters **3a,b**, powder X-ray diffraction patterns, and UV−visible spectra and particle size analyses for the residues remaining after solid-state thermolysis of clusters **2** and **3**. This material is available free of charge via the Internet at http://pubs.acs.org.

IC0481576